

# String Scattering and Evolution of Ryu-Takayanagi Surface

Xin Jiang, Houwen Wu and Haitang Yang

*College of Physics  
Sichuan University  
Chengdu, 610065, China*

domoki@stu.scu.edu.cn, iverwu@scu.edu.cn, hyanga@scu.edu.cn

## Abstract

In this paper, our aim is to illustrate that the process of open string scattering corresponds to the evolution of the entanglement wedge, where the scattering distance is identified as the entanglement wedge cross-section. Moreover, open-closed string scattering, specifically the disk-disk interaction, works for the evolution of the reflected entanglement wedge, with the circumference of the waist cross-section equating to the reflected entropy. It therefore provides evidence for the deep connections between the string worldsheet and the Ryu-Takayanagi surface. This connection is not only a coincidence rooted in hyperbolic geometry; it also reflects an additional correspondence between two distinct theories: mutual information and the geometric BV master equation.

# Contents

<b>1</b>	<b>Introduction</b>	<b>2</b>
<b>2</b>	<b>EWCS, reflected entropy and their phase transitions</b>	<b>5</b>
<b>3</b>	<b>Hyperbolic open and closed string vertices</b>	<b>7</b>
<b>4</b>	<b>Connections between string vertices and entanglement wedge evolution</b>	<b>12</b>
4.1	Correspondence between mutual information and the geometric BV equation . . . . .	13
4.2	Open-closed string scattering and reflected entanglement wedge evolution . . . . .	17
<b>5</b>	<b>Discussion and conclusion</b>	<b>19</b>

## 1 Introduction

The AdS/CFT correspondence plays a central role in modern theoretical physics. It conjectures that a weakly coupled gravitational theory in the bulk of  $\text{AdS}_{d+1}$  is equivalent to a strongly coupled  $d$  dimensional CFT on the conformally flat boundary [1]. It provides a testable realization for the holographic principle [2, 3]. One of the most successful supports for the AdS/CFT correspondence is the Ryu and Takayanagi (RT) formula, which asserts the equality of the entanglement entropy (EE) of the  $\text{CFT}_d$  and the accordingly defined minimal surface area in the bulk  $\text{AdS}_{d+1}$  [4–6]. In their work, the geodesic length (minimal surface area) in  $\text{AdS}_3$  is calculated and found in agreement with the EE of  $\text{CFT}_2$ . This identification is then verified extensively by follow-ups, referring to a recent review [7] and references therein. To quantify multipartite entanglement, the EE for a pure state becomes inadequate, requiring consideration of the entanglement of purification. Consequently, the bulk dual, represented by the RT surface, needs to be extended to include the entanglement wedges, entanglement wedge cross-sections (EWCS) and reflected surfaces.

In a recent work [8], we studied the connections between the hyperbolic string vertices of closed string field theory (CSFT) and the reflected surfaces. This connection arises from the fact that they are both subsets of hyperbolic geometry. And the critical length of hyperbolic geometry plays a central role in this connection. In CSFT, the main aim is to seek all consistent string vertices that integrate worldsheet correlators of string fields over specific regions of moduli spaces [9]. The construction of these vertices depends on how Riemann surfaces are coordinatized and how the corresponding parts of moduli spaces are covered. The consistency requires that the string vertices satisfy the geometric Batalin-Vilkoviski (BV) master equation. A recent development in constructing string vertices involves the introduction of hyperbolic geometry, providing a natural approach to understanding moduli space integration [10–12]. This result is soon generalized to hyperbolic open-closed

string vertices [13]. Further developments considering hyperbolic string vertices can be found in the following refs: [14–20]. To be specific, the hyperbolic three-string vertices in CSFT are constructed in three steps [12]:

1. Prepare two right-angled hexagons with side geodesic lengths  $L/2, \vartheta, L/2, \vartheta, L/2, \vartheta$ .
2. Glue two hexagons together along the geodesics  $\vartheta$ , giving the Y-piece  $\tilde{\mathcal{V}}_{0,3}(L)$ , which includes three geodesic boundaries with lengths  $(L/2) \times 2 = L$ .
3. Graft three flat semi-infinite cylinders with a circumference of  $L$  to the geodesic boundaries of  $\tilde{\mathcal{V}}_{0,3}(L)$  to obtain the three-string vertices  $\mathcal{V}_{0,3}(L)$ .

To satisfy the BV master equation, the boundary lengths of three-string vertices  $\mathcal{V}_{0,3}(L)$  are required to be  $L \leq L_* = \log(3 + 2\sqrt{2})$ . Furthermore, by gluing two Y-pieces  $\tilde{\mathcal{V}}_{0,3}(L)$  along the geodesic boundaries of length  $L$ , a new closed geodesic with length  $\delta$  is formed. These two simple geodesics intersect twice on the X-piece. When  $L \leq L_*$ , the critical length  $\delta$  always has a lower bound  $\delta > 2L_*$  which completely agrees with the lower bound of reflected entropy:  $S_R > 2L_*$  [21]. Based on this point, we can build an one-to-one correspondence between  $\delta$  and  $S_R$ . This consideration also works for open string field theory (OSFT). In OSFT, the critical length can be easily obtained for a single sheet of  $\tilde{\mathcal{V}}_{0,3}(L)$ .

However, these correspondences only connect the critical length and the value of reflected entropy. One might wonder whether we can further understand the relations between the string worldsheet and the evolved RT surface through these correspondences. Since string vertices are constructed within the unit Poincaré disk, we set the AdS radius  $\ell = 1$  for simplicity. In order to establish a connection between the properties of entanglement entropy and string vertices, we also make use of the "area law," which is inspired by holographic entanglement entropy. The entanglement entropy  $S_{EE}$  can be expressed as:

$$S_{EE} = \frac{L_{o/c}}{4G_N^{(3)}}, \quad (1.1)$$

where  $L_{o/c}$  represents the geodesic lengths obtained from the open or closed string vertices, respectively, and  $G_N^{(3)}$  is the 3-dimensional Newton constant. This relationship allows us to map geometric quantities from string theory to physical observables in the dual quantum theory, providing a direct connection between string theory and entanglement entropy via the holographic principle.

In this paper, our aim is to establish connections between the processes of string scattering and the evolution of RT surfaces. Specifically, we focus on specific RT surfaces in multipartite systems: the entanglement wedge which is surrounded by the RT surfaces, the EWCS and reflected surface. The EWCS, which serves as the bulk dual of entanglement of purification, measures entanglement entropy for mixed states [22]. When two entangled regions,  $A$  and  $B$ , are far apart, the EWCS vanishes, separating into two distinct systems. This well-known phase transition occurs at minimal EWCS  $E_W^{min}(\rho_{AB}) = \frac{c}{6} \log(3 + 2\sqrt{2}) = \frac{c}{6} L_*$  [22]. *In other words, the phase transition process is analogous to a scattering process where RT surfaces  $\gamma_C$  and  $\gamma_D$  interact to form  $\gamma_A$  and  $\gamma_D$ .* In OSFT, we have a similar process, where two open strings interact, transforming into another pair of open strings [23].

The scattering distance, obtained from hyperbolic string vertices, is also  $L_*$ . Thus, open string corresponds to the RT surface, open string scattering corresponds to the scattering of RT surfaces, and finally, the open string

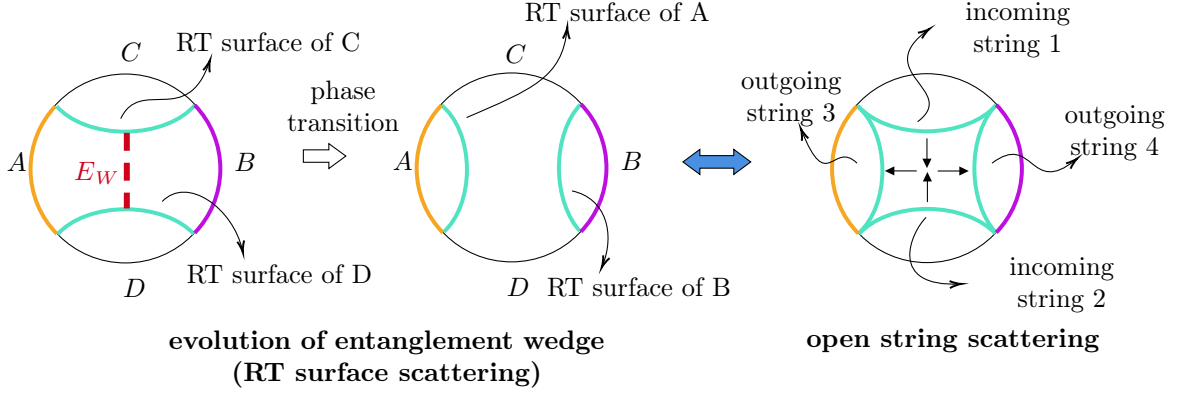


Figure 1: This picture roughly illustrates the correspondence between the RT surface scattering and open string scattering.

scattering distance is related to the EWCS by using (1.1), as roughly illustrated in figure (1). It is important to note that this correspondence is not only a coincidence rooted in hyperbolic geometry. It involves an additional connection between two distinct theories beyond hyperbolic geometry. In CSFT, hyperbolic string vertices are governed by two factors: hyperbolic geometry and the geometric BV master equation. Similarly, the phase transition in entanglement entropy depends on two components: hyperbolic geometry and mutual information. The link between hyperbolic string vertices and the phase transition in entanglement entropy arises from the relationship between the geometric BV master equation and mutual information, which are shown as follows:

$$\begin{array}{ccc}
 \boxed{\text{Phase transition of multipartite entanglement}} & = & \boxed{\text{Hyperbolic geometry} + \text{Mutual information}} \\
 \Downarrow & & \Downarrow \\
 \boxed{\text{Hyperbolic string vertices}} & = & \boxed{\text{Hyperbolic geometry} + \text{Geometric BV equation}}
 \end{array}$$

Both equations determine an equal boundary length for the X-piece, thereby sharing the same critical length,  $L_*$ . We will elaborate on this in the following sections.

On the other hand, canonical purification, another purification method, doubles and glues the original EWCS to yield the reflected entropy  $S_R$ , also serving as a measure of multipartite entanglement [21]. As expected,  $S_R(A, B) = 2E_W(\rho_{AB})$  for bipartite systems, with a transition point  $S_R^{min}(A, B) = \frac{c}{3}L_*$ . The phase transition process agrees perfectly with disk-disk interactions of open strings, resulting in a closed string cylinder. However, studying its relationship with open-closed string field theory poses a challenge. This is because the recent constructions for hyperbolic open-closed string vertices rely on flat disks and cylinders (a disk with a bulk puncture is equivalent to a flat circle with a marking, while an annulus without a puncture is represented as empty set [13]), whereas EWCS exhibits hyperbolic characteristics. To bridge this gap, we utilize open-closed string duality, revealing that a slice of disk-disk interaction corresponds to hyperbolic open string scattering. Therefore, its waist of hyperbolic cylinder can be calculated, measuring  $2L_*$ , corresponds to the reflected entropy. In short, these observations reveal deep connections between string scattering and the scattering of RT surfaces.

This paper is structured as follows: In Section 2, we provide a brief overview of the entanglement wedge cross-section, reflected entropy, and phase transitions. Section 3 offers a review of the fundamentals of hyperbolic open and closed string vertices. Section 4 establishes connections between string vertices and the evolution of the entanglement wedge and its reflected extension. The final section includes conclusions and discussions.

## 2 EWCS, reflected entropy and their phase transitions

In this section, we will review the EWCS, reflected entropy and their phase transitions. It is well-known that the traditional entanglement entropy (EE) serves as a measure of correlation between subsystems. In the simplest quantum system, pure state, the divided two subsystems can be denoted as  $A$  and  $B$ . The total Hilbert space is decomposed into  $\mathcal{H} = \mathcal{H}_A \otimes \mathcal{H}_B$ . By tracing out the degrees of freedom associated with the region  $B$ , a reduced density matrix for the region  $A$  can be derived, and denoted as  $\rho_A = \text{Tr}_{\mathcal{H}_B} \rho$ . The entanglement entropy of region  $A$  is then defined using the von Neumann entropy  $S_{EE}(A) = -\text{Tr}_{\mathcal{H}_A} (\rho_A \log \rho_A)$ , and we also have  $S_{EE}(A) = S_{EE}(B)$ . However, this method fails to measure the entanglement for mixed states, as the entanglement entropy of such states is always non-zero whether they are entangled or not. To solve this problem, one approach is to purify the mixed states and then introduce the entanglement of purification  $E_P$ , whose bulk dual is conjectured to be the area of the entanglement wedge cross-section  $E_W$ , specifically  $E_P = E_W/4G_N$ . For convenience, hereinafter, we set  $4G_N = 1$ . The computation of  $E_P$  is typically challenging as it requires minimizing over all possible purifications. To pass through this difficulty, an alternative method known as canonical purification has been proposed in [21], defining the reflected entropy  $S_R$ . This method is to copy the original mixed state as the purification. For a bipartite system, this identical copy is denoted as  $A^*B^*$ . The purified state and the reflected entropy are then defined as  $|\sqrt{\rho_{AB}}\rangle_{AA^*BB^*} = \sum_i \sqrt{p_i} |i\rangle_{AB} \otimes |i\rangle_{A^*B^*}$  and  $S_R(A : B) = S(AA^*)_{\sqrt{\rho_{AB}}} = -\text{Tr} \rho_{AA^*} \log \rho_{AA^*}$  where  $\rho_{AA^*} = \text{Tr}_{\mathcal{H}_{BB^*}} |\rho_{AB}\rangle \langle \rho_{AB}|$ . From the definition, it is easy to see  $S_R(A : B) = 2E_W(A : B)$ . The bulk interpretation of canonical purification is proposed in [24], which is referred as the reflected surface, also denoted as  $S_R$  to avoid confusion. Recently, we proposed a much simpler alternative for purification to measure the entanglements of mixed states [25].

In the rest of this section, we plan to introduce the bulk duals of the entanglement of purification and the canonical purification, which are denoted as EWCS and reflected surface separately. Moreover, we will also present the ingredient feature for these two purifications: connected and disconnected phase transitions.

**Entanglement wedge cross-section (EWCS) [22]:** Now, let us first review the EWCS based on [26]. Consider two subsystems,  $A$  and  $B$ , on the boundary without any overlap, see figure (2). The entanglement wedge  $M_{AB}$  is defined by a region whose boundary is given by:

$$\partial M_{AB} = A \cup B \cup \Gamma_{AB}^{min}, \quad (2.2)$$

where  $\Gamma_{AB}^{min}$  denotes the area of the minimal surface corresponding to the union  $A \cup B$ . Now, let us split the boundary of the entanglement wedge into two parts:

$$\partial M_{AB} = \tilde{\Gamma}_A \cup \tilde{\Gamma}_B, \quad (2.3)$$

where  $A \subset \tilde{\Gamma}_A$  and  $B \subset \tilde{\Gamma}_B$ . The holographic entanglement entropy is obtained by searching for the minimal surface  $\Sigma_{AB}^{min}$  which satisfies:

1.  $\partial\Sigma_{AB}^{min} = \partial\tilde{\Gamma}_A = \partial\tilde{\Gamma}_B$ ,
2.  $\Sigma_{AB}^{min}$  is homologous to  $\tilde{\Gamma}_A$  or  $\tilde{\Gamma}_B$ .

Then the EWCS is defined by the minimized area  $\Sigma_{AB}^{min}$  of all possible splits of the entanglement wedge:

$$E_W(A : B) = \min_{\tilde{\Gamma}_A \subset \partial M_{AB}} \left( \frac{A(\Sigma_{AB}^{min})}{4G_N} \right). \quad (2.4)$$

When two entangled regions,  $A$  and  $B$ , are far apart, the entanglement wedge cross-section vanishes, giving rise to two separate systems. This phenomenon represents a phase transition between the disconnected and connected phases. To see it clearly, let us consider it in a time slice of  $\text{AdS}_3$  and set the AdS radius to be unity. If we choose  $A = [a_1, a_2]$  and  $B = [b_1, b_2]$  where  $a_1 < a_2 < b_1 < b_2$ . The EWCS is given by:

$$E_W(A : B) = \frac{c}{6} \log \left( 1 + 2z + 2\sqrt{z(z+1)} \right), \quad (2.5)$$

and the corresponding mutual information is given by

$$I(A : B) = \frac{c}{3} \log z, \quad (2.6)$$

where  $z$  denotes the cross ratio:

$$z = \frac{(a_2 - a_1)(b_2 - b_1)}{(b_1 - a_2)(b_2 - a_1)} \geq 0. \quad (2.7)$$

when  $z \leq 1$ ,  $E_W(A : B) = I(A : B) = 0$ . Therefore, it gives a transition point at  $z = 1$ :

$$E_W^{min}(A : B) = \frac{c}{6} \log \left( 3 + 2\sqrt{2} \right). \quad (2.8)$$

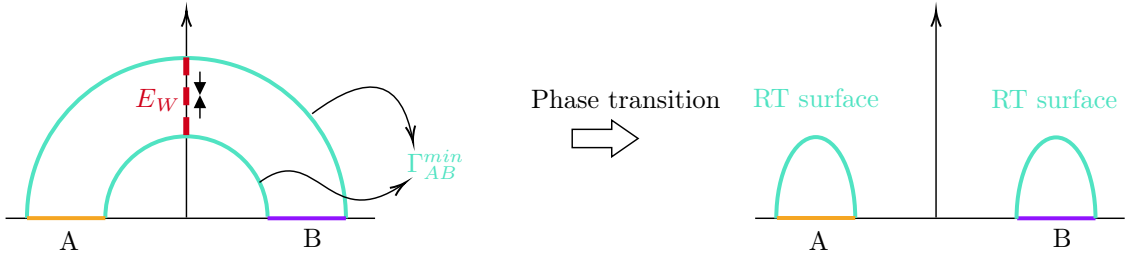


Figure 2: The entanglement wedge cross-section  $E_W(A, B)$  (red dashed line) is assumed to be a bulk dual of the entanglement of purification  $E_P(A, B)$  for bipartite mixed states. The essential ingredient is that there is a lower bound  $E_W^{min}(A, B)$  for the EWCS, due to the mutual information vanishing when  $A$  and  $B$  are distant. This lower bound indicates the phase transition point between the connected and disconnected entanglement wedges, transitioning from the left-hand side picture to the right-hand side picture.

**Reflected surface [21]:** The bulk dual of the reflected entropy is called reflected surface, which is also known as  $S_R$ . In the bulk interpretation, the reflected surface can be obtained by gluing two entanglement wedges

shown in figure (2) along the cyan geodesics, the result is shown in figure (3). As definition, the reflected surface is a closed simple geodesic, and it gives:

$$S_R(A : B) = 2E_W(A : B). \tag{2.9}$$

Due to the lower bound of  $E_W$ , there also exists a lower bound for  $S_R$ :

$$S_R^{min}(A : B) = 2E_W^{min}(A : B) = \frac{c}{3} \log(3 + 2\sqrt{2}). \tag{2.10}$$

In the rest of this paper, we will refer to the surface of this cylinder as the “reflected entanglement wedge” for simplicity.

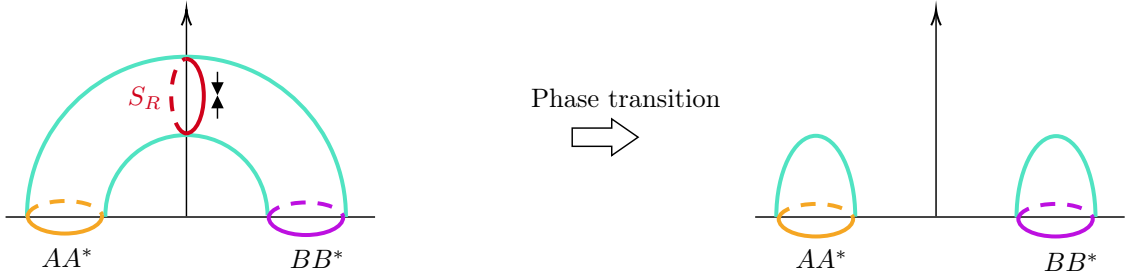


Figure 3: The phase transition of the reflected entanglement wedge is illustrated in the figure. The red circle, referred to as the reflected surface, with a length  $S_R$ , represents the bulk dual of reflected entropy. It comes from the copying and gluing of entanglement wedges. This surface is obtained through the copying and gluing of entanglement wedges. The lower bound of the EWCS also gives a lower bound for the reflected surface.

### 3 Hyperbolic open and closed string vertices

In this section, we aim to introduce the geometric BV master equation and its solution, known as string vertices, which are essential in open and closed string field theories. A good short review for the string field theory can be found in [27], on which our review is partially based. In string field theory, the string vertices play an important role since they are connected to off-shell amplitudes. These off-shell amplitudes can be derived from integrals over the moduli space of Riemann surfaces with genus  $g$  and  $n$  punctures. The correlation function in this integral is related to the states inserted at the punctures, which are not always  $(0, 0)$  conformal primaries. Local coordinate maps are therefore needed to map the punctured disk onto the Riemann surface, and the different choices of the coordinate maps represent different field redefinitions. The complete amplitudes resulted from summing all Feynman diagrams can be obtained by the gluing these string vertices and propagators. Therefore, the correct integration over the moduli space, without any overlapping or missing regions, is crucial for obtaining these amplitudes. And, this correct integration leads to the string vertices  $\mathcal{V}$  satisfying the geometric BV master equation:

$$\partial\mathcal{V} + \hbar\Delta\mathcal{V} + \frac{1}{2}\{\mathcal{V}, \mathcal{V}\} = 0, \tag{3.11}$$

where  $\mathcal{V}$  is a formal sum of string vertices associated to various moduli spaces  $\mathcal{V}_{g,n}$ ,  $\partial$  denotes the boundary operator acting on the moduli space,  $\Delta$  denotes to remove disks/semi-disks of two marked points on one

Riemann surface, and then twist-sewing the boundaries of these two disks/semi-disks.  $\{ , \}$  stands for removing two disks/semi-disks on two input Riemann surfaces respectively, and then twist-sewing them together [28, 29].

In the rest of this section, let us briefly review the recent development that construct string vertices using hyperbolic geometry.

At first, we introduce the Ultra-Parallel Theorem:

**Theorem 1** (Ultra-parallel theorem [30]) (Theorem 1.1.6): Any pair of ultra-parallel geodesics in the Poincaré disk has a unique perpendicular geodesics.

Following the Ultra-Parallel Theorem, it shows that there is a unique perpendicular line connecting any pair of boundary-anchored geodesics, see figure (4).

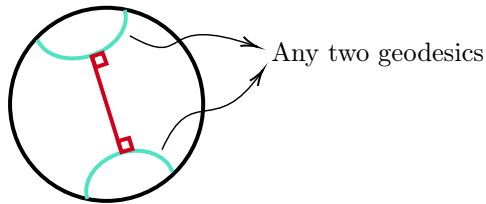


Figure 4: The red line denotes the shortest geodesic between any two cyan boundary-anchored geodesics. This red geodesic is perpendicular to the two cyan geodesics.

**Closed string vertices:** To construct the hyperbolic closed string vertices, we need to construct a Y-piece. The first step is to prepare a right-angled hexagon with side lengths  $L_c/2, \vartheta, L_c/2, \vartheta, L_c/2, \vartheta$ , see figure (5). This hexagon can be formed by plotting three boundary-anchored cyan geodesics  $\gamma_a = \gamma_b = \gamma_c$  in the Poincaré disk, where it is essential that the boundary regions have equal distances:  $a = b = c$  and  $A = B = C$ . From the ultra-parallel theorem, we can construct three unique perpendicular geodesics with lengths  $L_c/2$ , which are defined as the boundaries of the right-angled hexagon. The hexagon, as required, is enclosed by the cyan and red geodesics. Subsequently, we can copy this hexagon and then glue them along the cyan geodesics. The result is a pair-of-pants of boundary width  $L_c$ , known as a Y-piece or also called  $\tilde{\mathcal{V}}_{0,3}^c(L_c)$ . By grafting three semi-infinite cylinders of width  $L_c$ , we obtain a hyperbolic three-string vertex  $\mathcal{V}_{0,3}^c(L_c)$  in CSFT. The semi-infinite cylinders can be conformally mapped to the punctured disks, yielding a Riemann surface with markings.

**Open string vertices:** In figure (5), if we do not glue two hexagons together, the illustration represents the open string vertices  $\tilde{\mathcal{V}}_{0,3}^o(L_o)$  of OSFT with boundary lengths  $L_o = L_c/2$ . The open string vertices  $\mathcal{V}_{0,3}^o(L_o)$  is then obtained by grafting three semi-infinite strips on the boundaries of  $\tilde{\mathcal{V}}_{0,3}^o(L_o)$  of width  $L_o$ , see figure (6). The open string boundary conditions apply to the three cyan geodesics.

To satisfy the BV equation and construct the hyperbolic vertices, we need to introduce two essential ingredients: the **Collar theorem** and **systole**.

**Theorem 2** (Collar theorem [30]) (Theorem 4.1.1): Let  $\sigma_i$  be simple closed geodesics on a hyperbolic surface  $S$ , the collars:



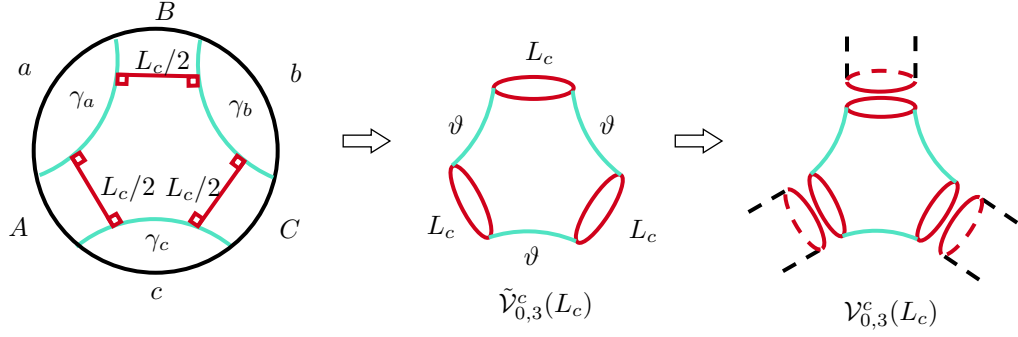


Figure 5: The construction for the closed string vertices.

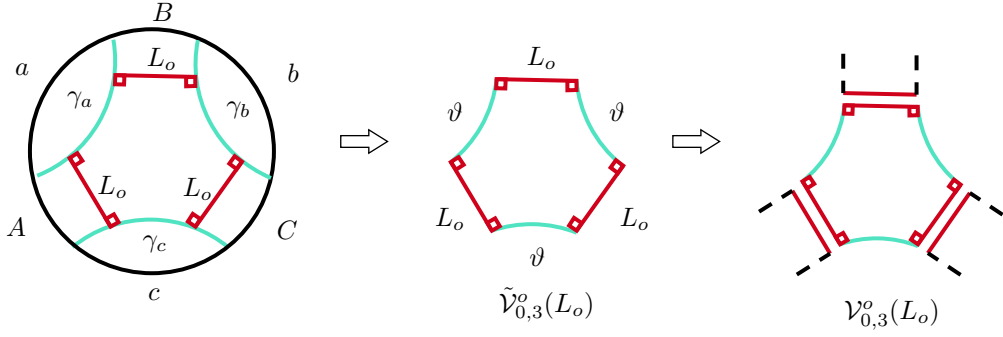


Figure 6: The construction for the open string vertices. Note that we can also view geodesics of lengths  $\vartheta$  as the boundaries of open string vertices  $\tilde{\mathcal{V}}_{0,3}^o(\vartheta)$ . Grafting three semi-infinite strips onto the boundaries of  $\tilde{\mathcal{V}}_{0,3}^o(\vartheta)$  with a width of  $\vartheta$  results in  $\mathcal{V}_{0,3}^o(\vartheta)$ . In this paper, for simplicity, we only consider  $L_o$  as the boundary.

$$\mathcal{C}(\sigma_i) = \left\{ p \in S \mid d(p, \sigma_i) \leq \frac{1}{2}\omega_i \right\}, \quad (3.12)$$

of widths  $\omega_i$

$$\sinh\left(\frac{1}{2}\omega_i\right) \sinh\left(\frac{1}{2}L_c(\sigma_i)\right) = 1, \quad (3.13)$$

are pairwise disjoint. We illustrate the simplest example in the left-hand side picture of figure (7). Based on the Collar theorem, for the open string worldsheet, the half-collars of the red boundaries with width  $L_o$  do not overlap with each other in figure (6).

From equation (3.13), a critical length can be defined for  $\omega_* = L_*$ , such that

$$L_* = 2 \operatorname{arcsinh}(1) = 2 \log(1 + \sqrt{2}) = \log(3 + 2\sqrt{2}). \quad (3.14)$$

Now, let us explain why the BV equation requires the Collar theorem. The gluing and cutting of string vertices require the geodesic boundaries to be minimal and equal. Based on the Collar theorem, if  $L_c \leq L_*$ , then the collar  $\omega \geq L_c$ . It ensures that the new closed geodesic (with length  $L' > \omega$ ) created by the sewing of two vertices

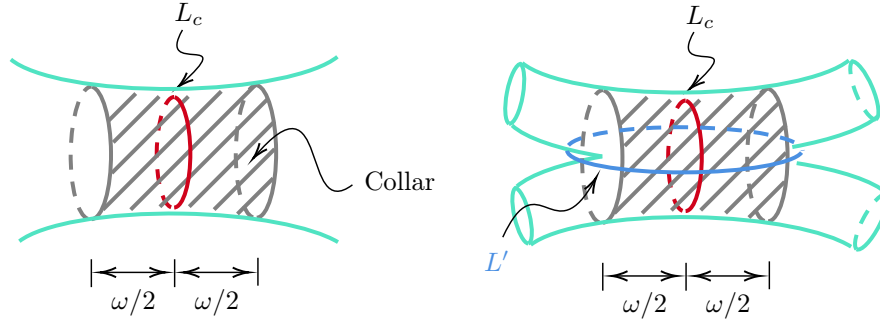


Figure 7: The left-side picture denotes the collar (shaded region) for the red geodesic of length  $L_c$ . Due to the Collar theorem, if we require the closed blue geodesic of length  $L'$  that emerges from sewing between two pairs of pants to be larger than  $L_c$ , we will obtain constraints for  $\omega$  and  $L_c$ :  $L' > \omega \geq L_c$ .

is always larger than  $L_c$  [12, 30], as shown in the right-hand side picture of figure (7) for example. Moreover, it also guarantees that any two simple geodesics (of lengths  $\leq L_*$ ) do not intersect with each other and give the fundamental building block.

Secondly, let us introduce the surfaces with systole:

**Systole:** The systole  $sys[\Sigma]$  of a surface  $\Sigma$  denotes the length of the shortest non-contractible closed geodesic that is not a boundary component.

The construction of hyperbolic string vertices  $\tilde{\mathcal{V}}_{g,n}(L)$  requires  $sys[\Sigma] \geq L$ , where  $L$  is the length of the boundary geodesics. In other words, there is no geodesic of length less than  $L$  on the surface of string vertices. This result guarantees that  $\partial\mathcal{V}_{g,n}(L)$  is the boundary of  $\mathcal{V}_{g,n}(L)$  in the moduli space, as seen in the two pictures on the right-hand side of figures (8) and (9).

Using these results, K. Costello and B. Zwiebach [12] established the following results in CSFT for the closed string interaction:

1. The sets of closed string vertices  $\mathcal{V}_{g,n}^c(L_c)$  of width  $L_c \leq L_*$  and  $sys[\tilde{\Sigma}_c] \geq L_c$  satisfy the quantum geometric master equation.
2. The closed string vertices  $\mathcal{V}_{g,n}^c(L_c)$  of width  $L_c > 0$  and  $sys[\tilde{\Sigma}_c] \geq L_c$  fulfill the classical geometric master equation (corresponding to  $\hbar \rightarrow 0$  in the BV equation), and they corresponds to classical hyperbolic CSFT.

In OSFT, there are similar results:

1. The sets of open string vertices  $\mathcal{V}_{g,n}^o(L_o)$  of width  $L_o \leq \frac{L_*}{2}$  and  $sys[\tilde{\Sigma}_o] \geq L_o$  meet the quantum geometric master equation.
2. The open string vertices  $\mathcal{V}_{g,n}^o(L_o)$  of width  $L_o > 0$  and  $sys[\tilde{\Sigma}_o] \geq L_o$  satisfy the classical geometric master equation.

The hyperbolic open string vertices can be defined by analogy to the closed string vertices:

$$\tilde{\mathcal{V}}_{g,n}^o(L_o) \equiv \left\{ \tilde{\Sigma}_o \in \mathcal{M}_{g,n,L_o} \mid \text{sys} \left[ \tilde{\Sigma}_o \right] \geq L_o \right\}, \quad (3.15)$$

where  $\mathcal{M}_{g,n,L_o}$  denotes the moduli space of genus  $g$  surfaces with  $n$  open string legs of length  $L_o$ . The open string vertices  $\mathcal{V}_{g,n}^o(L_o)$  are constructed by grafting flat  $n$  semi-infinite strips onto the punctures.

It is important to note that the BV master equation requires that both open string and closed string vertices possess boundaries of the same geodesic lengths. To illustrate this concept, let us refer to figures (8) and (9). We start with  $\mathcal{V}_{0,3}^c(L_c)/\mathcal{V}_{0,3}^o(L_o)$  and its copy, where the three outer boundaries of  $\mathcal{V}_{0,3}^c(L_c)/\mathcal{V}_{0,3}^o(L_o)$  have lengths  $L_c/L_o$ . By attaching two  $\mathcal{V}_{0,3}^c(L_c)/\mathcal{V}_{0,3}^o(L_o)$  together, we create the boundary of the moduli space  $\partial\mathcal{V}_{0,4}^c(L_c)/\partial\mathcal{V}_{0,4}^o(L_o)$ , indicating that all inner and outer boundaries have the same length  $L_c/L_o$ . If we were to relax the length of the inner boundary to an arbitrary value  $2L_i/L_i$  that satisfies the systole requirements, the result is  $\mathcal{V}_{0,4}^c(L_c)/\mathcal{V}_{0,4}^o(L_o)$ .

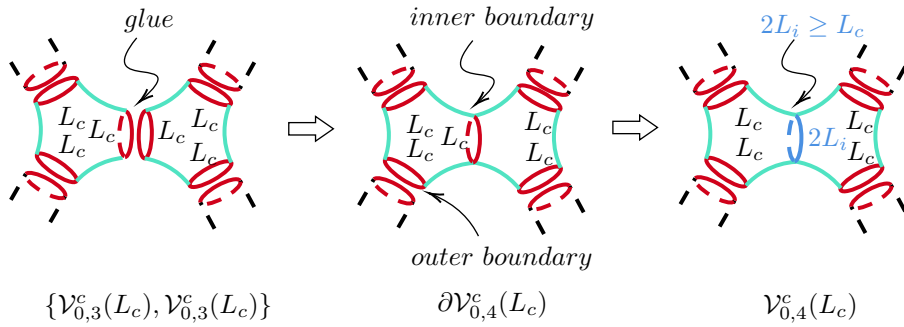


Figure 8: The gluing of two closed string vertices occurs when all outer and inner boundaries have equal lengths. It denotes the boundary of vertices  $\partial\mathcal{V}_{0,4}^c(L_c)$  in the moduli space. The construction requires the systole  $\text{sys} \left[ \tilde{\mathcal{V}}(L_c) \right] \geq L_c$  for the vertices  $\mathcal{V}_{0,4}^c(L_c)$ , and it can be roughly seen as  $2L_i \geq L_c$  in the last picture.

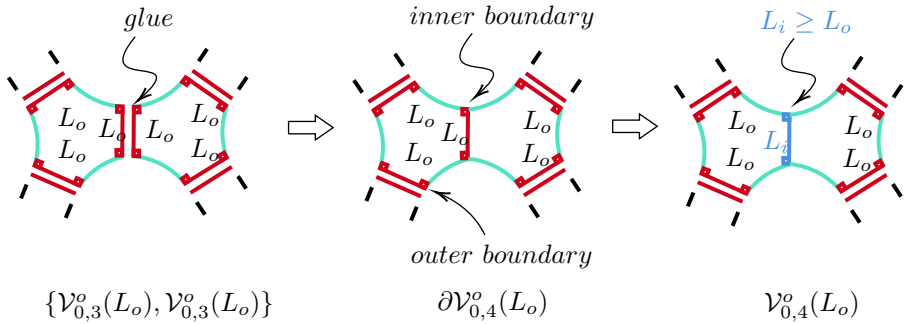


Figure 9: The gluing of two open string vertices occurs when all outer and inner boundaries have equal lengths. It denotes the boundary of vertices  $\partial\mathcal{V}_{0,4}^o(L_o)$  in the moduli space. The construction requires the systole  $\text{sys} \left[ \tilde{\mathcal{V}}(L_o) \right] \geq L_o$  for the vertices  $\mathcal{V}_{0,4}^o(L_o)$ , and it can be roughly seen as  $L_i \geq L_o$  in the last picture.

## 4 Connections between string vertices and entanglement wedge evolution

In this section, we plan to figure out the relations between phase transition of entanglement wedge and string vertices.

Let us first revisit figure (2), which illustrates the entanglement wedge bounded by the RT surfaces between  $A$  and  $B$ . When the EWCS reaches its minimal value  $E_W^{min}(A, B)$ , the entanglement wedge vanishes and transforms into two separate RT surfaces. This process is very similar to the four open strings scattering: when two open strings interact, they give another pair of open strings. Moreover, in the theory of hyperbolic open string vertices, this minimal value can be understood as a scattering distance, indicating that interaction occurs only when the width reaches a critical length. In figure (10), we show two types of interactions between open strings: the top-down interaction introduces the critical length  $L_{AB}$ , and the left-right interaction provides the critical length  $L_{CD}$ .

By plotting these processes involving RT surfaces and open strings in the Poincaré disk, we obtain two similar configurations: hyperbolic ideal quadrilaterals with mutually perpendicular geodesics, as shown in figure (11). Our goal is to verify whether these two configurations are indeed identical, specifically:

$$E_{AB}^{min} \stackrel{?}{=} L_{AB}^{min}, \quad \text{and} \quad E_{CD}^{min} \stackrel{?}{=} L_{CD}^{min}. \quad (4.16)$$

Note the EWCS is defined as  $E_W(A, B) = E_{AB}/4G_N^{(3)}$ . However, this equivalence cannot be obtained based only on hyperbolic geometry, as it provides the geodesics but not their specific lengths. To establish a connection between the lengths in the two theories, a deeper investigation into their correspondence is required. *Fortunately, we find that mutual information is related to the geometric BV master equation, bridging this gap.*

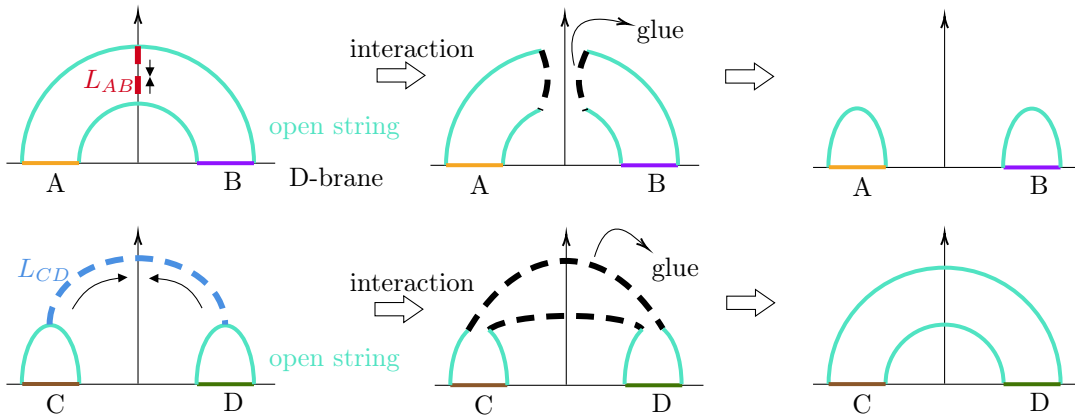


Figure 10: These pictures demonstrate the two types of open string interactions. When two open strings interact with each other, they break at the mid-point and then glue to the other half of the string. Here,  $L_{AB}$  and  $L_{CD}$  denote the distances between the two open strings.

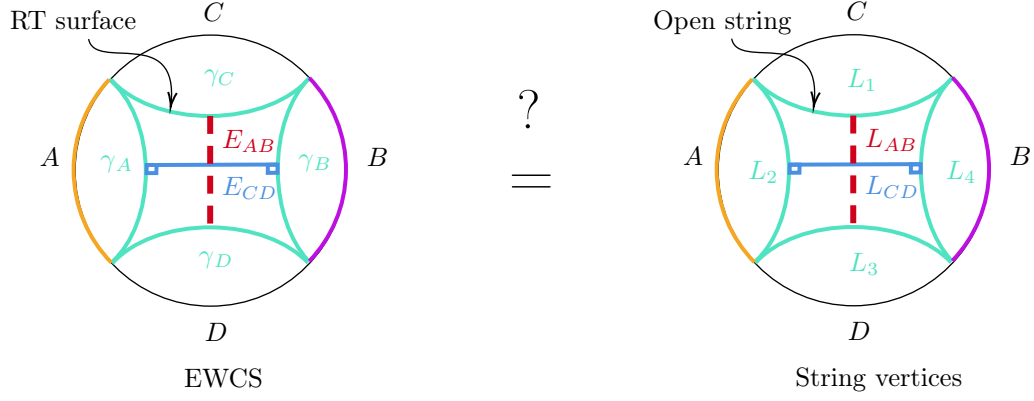


Figure 11: The left-hand side image depicts the quadrilateral resulting from the phase transition of the EWCS, where  $\gamma_i$  represents the RT surface, and  $E_{AB/CD}$  denotes the geodesic length between the RT surfaces. The right-hand side image illustrates the quadrilateral formed by open string vertices, where  $L_i$  represents the boundary of the string vertices, and  $L_{AB/CD}$  is the scattering distance (geodesic length between open strings).

## 4.1 Correspondence between mutual information and the geometric BV equation

### Mutual information

Let us first consider the mutual information

$$I(A : B) = S_A + S_B - S_{A \cup B}, \quad (4.17)$$

where  $S_A$ ,  $S_B$ , and  $S_{A \cup B}$  denote the entanglement entropies of regions  $A$ ,  $B$ , and the combined region  $A \cup B$ , respectively. If we represent the remaining regions of the system as  $C$  and  $D$ , the mutual information can also be expressed as

$$I(A : B) = S_A + S_B - (S_C + S_D). \quad (4.18)$$

The sub-additivity condition guarantees that  $I(A : B) \geq 0$ , which implies:

$$S_A + S_B \geq S_C + S_D. \quad (4.19)$$

Conversely,  $I(C : D)$  becomes relevant when

$$S_A + S_B \leq S_C + S_D. \quad (4.20)$$

A phase transition occurs at the point where

$$S_A + S_B = S_C + S_D. \quad (4.21)$$

This phase transition is illustrated in figure (12).

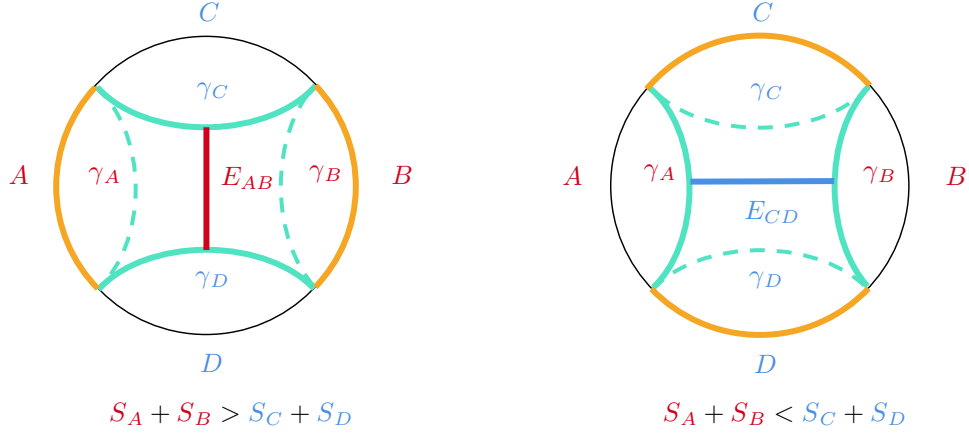


Figure 12: The left-hand side image depicts the entanglement wedge enclosed by regions  $A$ ,  $B$ ,  $\gamma_C$  and  $\gamma_D$ , which exists only when  $S_A + S_B \geq S_C + S_D$ . The corresponding EWCS is given by  $E_W(A : B) = E_{AB}/4G_N^{(3)}$ . In contrast, the right-hand side image shows the entanglement wedge when  $S_A + S_B \leq S_C + S_D$ , enclosed by regions  $C$ ,  $D$ ,  $\gamma_A$  and  $\gamma_B$ . The corresponding EWCS is expressed as  $E_W(C : D) = E_{CD}/4G_N^{(3)}$ .

To see how this equivalence (4.21) imposes an additional constraint on the hyperbolic ideal quadrilaterals shown in the left-hand side of figure (11), we recall the bipartite mixed state in the holographic framework, where the entanglement entropy  $S_i$  is given by the geodesic length of  $\gamma_i$  in the hyperbolic Poincaré disk:

$$S_{EE} = \frac{\text{Area}(\gamma_i)}{4G_N^{(3)}}. \quad (4.22)$$

From this holographic derivation, the equation  $S_A + S_B = S_C + S_D$  translates to  $\gamma_A + \gamma_B = \gamma_C + \gamma_D$ . To calculate the transition point determined by this equation, we must consider a configuration involving four right-angled pentagons, as shown in figure (13).

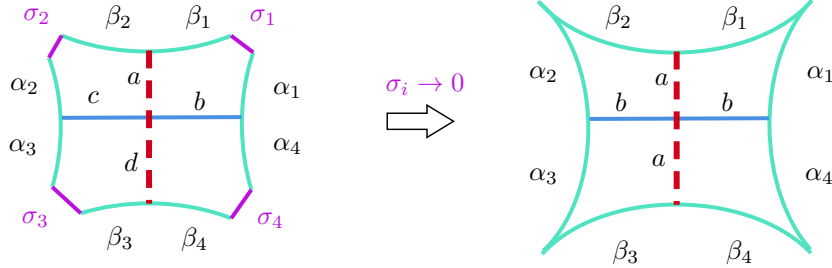


Figure 13: Hyperbolic ideal quadrilaterals can be constructed by gluing together four pentagons and setting the four boundary parameters  $\sigma_i$  to zero.

For the pentagon in the upper right corner, we have the relation ([30], Theorem 2.3.4 (i)):

$$\cosh \sigma_1 = \sinh a \sinh b. \quad (4.23)$$

As  $\sigma_1 \rightarrow 0$ , this simplifies to:

$$\sinh a \sinh b = 1. \quad (4.24)$$

Similarly, as  $\sigma_2, \sigma_3, \sigma_4 \rightarrow 0$ , we obtain:

$$\begin{aligned} \sinh a \sinh c &= 1, \\ \sinh c \sinh d &= 1, \\ \sinh d \sinh b &= 1. \end{aligned} \quad (4.25)$$

For the hyperbolic quadrilateral, we thus have:

$$b = c, \quad a = d. \quad (4.26)$$

When  $\sigma_i \rightarrow 0$ , the right-angled pentagons reduce to trirectangles. For the trirectangles in the upper right corner, we have ([30], Theorem 2.3.1 (iv)):

$$\tanh \beta_1 = \frac{\cosh a}{\coth b}, \quad \tanh \alpha_1 = \frac{\cosh b}{\coth a}. \quad (4.27)$$

Similarly, we find:

$$\begin{aligned} \tanh \beta_2 &= \frac{\cosh a}{\coth b}, & \tanh \alpha_2 &= \frac{\cosh b}{\coth a}, \\ \tanh \beta_3 &= \frac{\cosh a}{\coth b}, & \tanh \alpha_3 &= \frac{\cosh b}{\coth a}, \\ \tanh \beta_4 &= \frac{\cosh a}{\coth b}, & \tanh \alpha_4 &= \frac{\cosh b}{\coth a}. \end{aligned} \quad (4.28)$$

Therefore, the transition point where  $\gamma_A + \gamma_B = \gamma_C + \gamma_D$  requires

$$(\alpha_2 + \alpha_3) + (\alpha_1 + \alpha_4) = (\beta_2 + \beta_1) + (\beta_3 + \beta_4). \quad (4.29)$$

For  $a, b \geq 0$ , using (4.28) and (4.29), we obtain:

$$a = b = \frac{1}{2} \log(3 + 2\sqrt{2}), \quad \alpha_i = \beta_i \quad (4.30)$$

In summary, the transition point of mutual information imposes an additional constraint on the hyperbolic geometry, such that

$$\gamma_A = \gamma_B = \gamma_C = \gamma_D, \quad \text{and} \quad E_{AB}^{min} = E_{CD}^{min} = \log(3 + 2\sqrt{2}), \quad (4.31)$$

in the quadrilateral. This result corresponds exactly to the minimal EWCS [22].

## Geometric BV master equation

On the other hand, let us examine how the geometric BV master equation imposes an additional constraint on the hyperbolic quadrilateral shown on the right-hand side of figure (11), leading to the determination of the critical length. We begin by transforming the four open strings scattering (shown in figure (10)) into hyperbolic four-string vertices. The entire process can be seen as the joining and splitting of two segments of three-open string vertices, namely  $\{\mathcal{V}_{0,3}^o(L_o), \mathcal{V}_{0,3}^o(L_o)\}$ , or  $\mathcal{V}_{0,4}^o(L_o)$ . To match this process with the phase transition picture of the the EWCS,  $\mathcal{V}_{0,4}^o(L_o)$  should have a large  $L_o$ . Therefore, our goal is to calculate  $L_{AB}$  and  $L_{CD}$  for the string vertices  $\mathcal{V}_{0,4}^o(L_o)$ , as illustrated in figure (14).

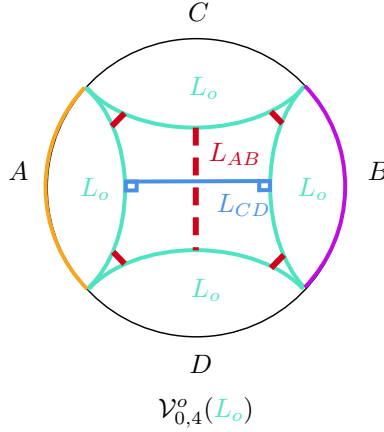


Figure 14: Based on the hyperbolic four-string vertices, there exists a minimal value for  $L_{AB}$  or  $L_{CD}$ . It gives the scattering distance. It also indicates the transition point between the top-down cyan geodesics and the left-hand cyan geodesics.

Now, let us revisit the requirements of the geometric BV master equation, as derived in the previous section:

The open string vertices  $\mathcal{V}_{g,n}^o(L_o)$  of width  $L_o > 0$  and  $\text{sys}[\tilde{\mathcal{V}}(L_o)] \geq L_o$  satisfy the classical geometric master equation.

To satisfy the classical BV equation (where there are no loops in the correspondence), the four cyan boundaries must all be of equal length, namely  $L_1 = L_2 = L_3 = L_4 = L_o$ . In hyperbolic geometry, this requirement gives  $L_{AB} = L_{CD}$ . Recall the hexagon: when the four outer red boundaries approach zero, the two inner geodesics  $L_{AB}$  and  $L_{CD}$  satisfy the following equality ([30], Theorem 2.3.1 (i)):

$$\sinh\left(\frac{L_{AB}}{2}\right) \sinh\left(\frac{L_{CD}}{2}\right) = 1. \quad (4.32)$$

This equation provides the minimal critical length, which is given by  $L_{AB}^{min} = L_{CD}^{min} = L_*$ :

$$L_* = 2 \text{arc sinh}(1) = 2 \log(1 + \sqrt{2}) = \log(3 + 2\sqrt{2}). \quad (4.33)$$

Thus, the geometric BV master equation imposes an additional constraint on the hyperbolic quadrilateral, resulting in:



$$L_1 = L_2 = L_3 = L_4 = L_o, \quad \text{and} \quad L_{AB}^{min} = L_{CD}^{min} = L_* = \log\left(3 + 2\sqrt{2}\right), \quad (4.34)$$

in the quadrilateral.

Finally, by comparing the results from mutual information (4.31) and the geometric BV master equation (4.34), we can confirm that the hyperbolic quadrilaterals in both theories, as shown in figure (11), are identical. Thus, we arrive at the following:

$$E_{AB}^{min} = L_{AB}^{min} = L_*, \quad \text{and} \quad E_{CD}^{min} = L_{CD}^{min} = L_*. \quad (4.35)$$

This result implies that the correspondence between the EWCS and string vertices is not only a coincidence arising from hyperbolic geometry but is obtained by the extra relation between mutual information and geometric BV master equation of two theories. Thus, the EWCS and string vertices are directly related based on the observation:

$$E_W^{min}(A : B/C : D) = \frac{E_{AB/CD}^{min}}{4G_N^{(3)}} = \frac{L_*}{4G_N^{(3)}} = \frac{c}{6} \log\left(3 + 2\sqrt{2}\right), \quad (4.36)$$

where the last equivalence follows from the fact that  $c = 3/2G_N^{(3)}$ . Therefore, the following connections can be established:

- Open string scattering corresponds to the evolution of the entanglement wedge.
- The open string scattering distance  $L_{AB/CD}^{min}$  relates to the entanglement wedge cross-section (EWCS)  $E_W^{min}(A : B/C : D)$ .

## 4.2 Open-closed string scattering and reflected entanglement wedge evolution

In addition to the connection between entanglement wedge and open string interaction, there is also a connection to the reflected entropy. As expected, the closed string vertices enter the story. In this subsection, we wish to include the reflected entropy in our framework. Let us recall figure (3), which demonstrates the reflected geometry obtained through copying and gluing the original entanglement wedge. The EWCS is thus doubled and called the reflected surface. When the reflected surface reaches its minimal value  $S_R^{min}(A, B)$ , the corresponding reflected geometry vanishes and transforms into two separate RT surfaces. This process can be seen as the interaction between two open string disks. During this process, the two open string disks interact with each other, transforming into the closed string cylinder, as shown in figure (15).

The entire process, which can be seen as the joining of two segments of open string disks and yielding a closed string cylinder, is illustrated in figure (16).

However, there is no well-defined open-closed string vertices to describe this process. The reason is that, in the recent construction of hyperbolic open-closed string vertices, the open string disk without boundary punctures is flat. The interaction between two flat disks results in a flat cylinder. This implies that it is difficult to establish a clear connection between this process and the hyperbolic entanglement wedge. To solve this problem, we can utilize the open-closed string duality. This duality reveals that a closed string cylinder can be

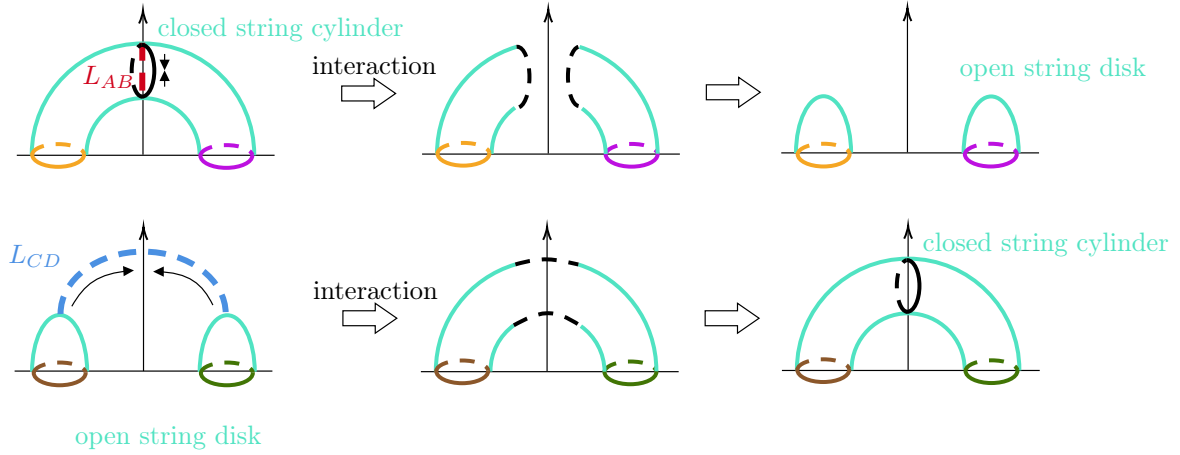


Figure 15: These pictures illustrate the disk-disk interactions. In the first row, the center of the closed string cylinder contracts and then breaks into two open string disks. The second row shows how the two open string disks interact with each other and transform into a closed string cylinder.

identified as a one-loop of open string. In other words, we can take the time-slice of this picture, corresponding to open string scattering. This open string scattering can be described by the previous hyperbolic open string vertices, as shown in (14).

Now, let us calculate the length  $L_c$  and compare it with the reflected entropy  $S_R$ . Before calculation, it is essential to clarify a point. In figure (16), if the waist cross-section<sup>1</sup> of a cylinder is a perfect circle, we will have:

$$L_2 = \pi L_1, \quad L_c = \pi L_{AB}. \quad (4.37)$$

However, if we consider this process in the Poincaré disk (see figure (17)), there is a problem: the corresponding boundary entangling regions  $L_2/2$  (in reflected entropy, this region of length  $L_2$  is obtained by gluing two entanglement wedges of boundary lengths  $L_2/2$ , see figure (3)) and  $L_1$  are not equal. It implies that the result is inconsistent with multipartite entanglement: when we take a slice of the reflected entanglement wedge, it can be seen as a new entanglement wedge. The corresponding EWCS and reflected entropy must vanish simultaneously. In other words, they must have the same entangling regions. However, if  $L_2/2 < L_1$ , the EWCS  $E_W(A, B)$  will vanish before the reflected entropy  $S_R(A, B)$ , which corresponds to different entangling regions. Therefore, to solve this problem, the waist cross-section of the cylinder cannot be a perfect circle, and there is a requirement:  $L_2/2 \rightarrow L_1$ . Then, we will obtain the following result:

$$L_c = 2L_{AB} \leq 2L_*, \quad (4.38)$$

where  $L_{CD} \geq L_*$ , or vice versa. This result is precisely equivalent to the minimal reflected entropy (3) [21]. In other words, there will always be one non-vanishing EWCS between  $AB$  or  $CD$ , and its size is greater than:

$$S_R^{min}(A : B/C : D) = \frac{c}{3} \log \left( 3 + 2\sqrt{2} \right) = \frac{2L_*}{4G_N^{(3)}}, \quad (4.39)$$

<sup>1</sup>In this subsection, the term 'waist cross-section' refers to the cross-section of the narrowest part of a hyperbolic cylinder.

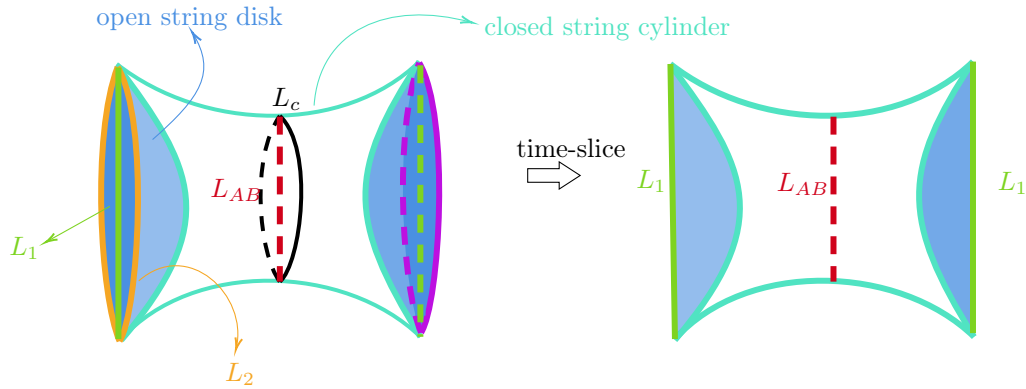


Figure 16: The entire process of disk-disk interaction is illustrated in the left-hand side picture. Due to open-closed string duality, taking a slice of the left-hand side picture results in the right-hand side, representing open string scattering. The orange and purple circles on the boundary have lengths  $L_2$ , and the black circle in the middle has a length  $L_c$ . If they are perfect circles, the green and red lines, with lengths  $L_1$  and  $L_{AB}$  respectively, represent their diameters.

In short, we present the following connections in this subsection:

- Disk-disk string scattering corresponds to the evolution of reflected entanglement wedge.
- Circumference of disk-disk scattering waist cross-section  $L_c$  corresponds to the reflected surface/entropy  $S_R$ .

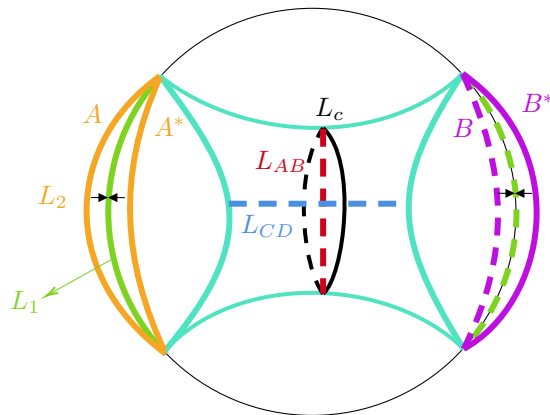


Figure 17: Disk-disk scattering in the Poincaré disk. To establish a connection between entanglement entropy, the EWCS, and the reflected surface in this scenario, should be the bulk duals for the bipartite entanglement entropy corresponding to the same entangling regions  $A$  and  $B$ . This implies that  $L_1$  and  $L_2/2$  must have the same value.

## 5 Discussion and conclusion

In summary, we have established connections between string scattering and the evolution of RT surfaces in the context of multipartite entanglement. For open string field theory, we demonstrated that open string scattering

corresponds to the evolution of the entanglement wedge, and the width of the open string scattering distance relates to the EWCS. In open-closed string field theory, by taking a slice of open-closed string vertices described by hyperbolic open string vertices, we observed that disk-disk interaction corresponds to hyperbolic open string scattering. The circumference of its waist cross-section corresponds to the reflected entropy.

Some remarks and future works are as follows:

- In SFT, the calculation of string scattering amplitudes using marked Riemann surfaces requires attaching semi-infinite flat strips or cylinders to open or closed boundaries of vertices. These structures can be conformally mapped to the punctured disk or semi-disk. However, in holographic entanglement entropy, hyperbolic strips and cylinders play a crucial role, as they can be glued to the boundaries of Y-piece or hexagon. The connections between hyperbolic string vertices and entanglement entropy motivates us to investigate whether building blocks of string field theory can be constructed using hyperbolic strips and cylinders.
- Based on the relationships between string scattering and the evolution of RT surface, it is conceivable to explore whether the entanglement entropy can be derived from the off-shell string amplitude, or vice versa.

**Acknowledgements** This work is supported in part by NSFC (Grant No. 12105191, 12275183 and 12275184).

## References

- [1] J. M. Maldacena, “The Large N limit of superconformal field theories and supergravity,” *Int. J. Theor. Phys.* **38**, 1113 (1999) [*Adv. Theor. Math. Phys.* **2**, 231 (1998)] doi:10.1023/A:1026654312961 [hep-th/9711200].
- [2] G. ’t Hooft, “Dimensional reduction in quantum gravity,” *Salamfest 1993:0284-296* [gr-qc/9310026].
- [3] L. Susskind, “The World as a hologram,” *J. Math. Phys.* **36**, 6377 (1995) doi:10.1063/1.531249 [hep-th/9409089].
- [4] S. Ryu and T. Takayanagi, “Holographic derivation of entanglement entropy from AdS/CFT,” *Phys. Rev. Lett.* **96**, 181602 (2006) doi:10.1103/PhysRevLett.96.181602 [hep-th/0603001].
- [5] S. Ryu and T. Takayanagi, “Aspects of Holographic Entanglement Entropy,” *JHEP* **0608**, 045 (2006) doi:10.1088/1126-6708/2006/08/045 [hep-th/0605073].
- [6] V. E. Hubeny, M. Rangamani and T. Takayanagi, “A Covariant holographic entanglement entropy proposal,” *JHEP* **0707**, 062 (2007) doi:10.1088/1126-6708/2007/07/062 [arXiv:0705.0016 [hep-th]].
- [7] M. Rangamani and T. Takayanagi, “Holographic Entanglement Entropy,” arXiv:1609.01287 [hep-th].
- [8] P. Wang, H. Wu and H. Yang, “Connections between reflected entropies and hyperbolic string vertices,” *JHEP* **05**, 127 (2022) doi:10.1007/JHEP05(2022)127 [arXiv:2112.09503 [hep-th]].

- [9] B. Zwiebach, “Closed string field theory: Quantum action and the B-V master equation,” Nucl. Phys. B **390**, 33 (1993) doi:10.1016/0550-3213(93)90388-6 [hep-th/9206084].
- [10] S. F. Moosavian and R. Pius, “Hyperbolic geometry and closed bosonic string field theory. Part I. The string vertices via hyperbolic Riemann surfaces,” JHEP **08**, 157 (2019) doi:10.1007/JHEP08(2019)157 [arXiv:1706.07366 [hep-th]].
- [11] S. F. Moosavian and R. Pius, “Hyperbolic geometry and closed bosonic string field theory. Part II. The rules for evaluating the quantum BV master action,” JHEP **08**, 177 (2019) doi:10.1007/JHEP08(2019)177 [arXiv:1708.04977 [hep-th]].
- [12] K. Costello and B. Zwiebach, “Hyperbolic string vertices,” JHEP **02**, 002 (2022) doi:10.1007/JHEP02(2022)002 [arXiv:1909.00033 [hep-th]].
- [13] M. Cho, “Open-closed Hyperbolic String Vertices,” JHEP **05**, 046 (2020) doi:10.1007/JHEP05(2020)046 [arXiv:1912.00030 [hep-th]].
- [14] A. H. Firat, “Hyperbolic three-string vertex,” JHEP **08** (2021), 035 doi:10.1007/JHEP08(2021)035 [arXiv:2102.03936 [hep-th]].
- [15] N. Ishibashi, “The Fokker–Planck formalism for closed bosonic strings,” PTEP **2023**, no.2, 023B05 (2023) doi:10.1093/ptep/ptad014 [arXiv:2210.04134 [hep-th]].
- [16] H. Erbin and A. H. Firat, “Characterizing 4-string contact interaction using machine learning,” [arXiv:2211.09129 [hep-th]].
- [17] A. H. Firat, “Bootstrapping closed string field theory,” JHEP **05**, 186 (2023) doi:10.1007/JHEP05(2023)186 [arXiv:2302.12843 [hep-th]].
- [18] A. H. Firat, “Hyperbolic string tadpole,” SciPost Phys. **15**, no.6, 237 (2023) doi:10.21468/SciPostPhys.15.6.237 [arXiv:2306.08599 [hep-th]].
- [19] H. Erbin and A. H. Firat, “Open string stub as an auxiliary string field,” [arXiv:2308.08587 [hep-th]].
- [20] A. H. Firat, “String vertices for the large  $N$  limit,” [arXiv:2311.00747 [hep-th]].
- [21] S. Dutta and T. Faulkner, “A canonical purification for the entanglement wedge cross-section,” JHEP **03** (2021), 178 doi:10.1007/JHEP03(2021)178 [arXiv:1905.00577 [hep-th]].
- [22] T. Takayanagi and K. Umemoto, “Entanglement of purification through holographic duality,” Nature Phys. **14**, no.6, 573-577 (2018) doi:10.1038/s41567-018-0075-2 [arXiv:1708.09393 [hep-th]].
- [23] E. Witten, “Noncommutative Geometry and String Field Theory,” Nucl. Phys. B **268**, 253-294 (1986) doi:10.1016/0550-3213(86)90155-0
- [24] N. Engelhardt and A. C. Wall, “Coarse Graining Holographic Black Holes,” JHEP **05** (2019), 160 doi:10.1007/JHEP05(2019)160 [arXiv:1806.01281 [hep-th]].

- [25] X. Jiang, P. Wang, H. Wu and H. Yang, “An alternative to purification in CFT,” [arXiv:2406.09033 [hep-th]].
- [26] N. Jokela and A. Pönni, “Notes on entanglement wedge cross sections,” JHEP **07**, 087 (2019) doi:10.1007/JHEP07(2019)087 [arXiv:1904.09582 [hep-th]].
- [27] C. Maccaferri, “String Field Theory,” [arXiv:2308.00875 [hep-th]].
- [28] A. Sen and B. Zwiebach, “Quantum background independence of closed string field theory,” Nucl. Phys. B **423**, 580 (1994) doi:10.1016/0550-3213(94)90145-7 [hep-th/9311009].
- [29] A. Sen and B. Zwiebach, “Background independent algebraic structures in closed string field theory,” Commun. Math. Phys. **177**, 305 (1996) doi:10.1007/BF02101895 [hep-th/9408053].
- [30] P. Buser, “Geometry and spectra of compact Riemann surfaces,” Birkhauser Boston 1992.